UNIVERSITYOF BIRMINGHAM

Stable iron isotopic composition of atmospheric aerosols

Wang, Yuantao; Wu, Libin; Hu, Wei; Li, Weijun; Shi, Zongbo; Harrison, Roy M.; Fu, Pingqing

[Link to publication on Research at Birmingham portal](#)

REVIEW ARTICLE   OPEN

Stable iron isotopic composition of atmospheric aerosols: An overview

Yuantao Wang [1,5], Libin Wu[1,5], Wei Hu [1], Weijun Li [2], Zongbo Shi [3], Roy M. Harrison [3,4] and Pingqing Fu[1] ✉

Atmospheric particulate matter (PM) has a significant impact on both the natural environment and human health. Iron is one of the most abundant elements in the earth's crust, playing an important role in geochemical processes, and is also an important trace component in atmospheric PM. In recent years, with the rapid development of non-traditional (metal) stable isotope technologies, new solutions and methods for the source apportionments of heavy metal elements have been put forward. Stable iron isotope analysis has become an effective tool to trace iron in atmospheric particles. This review paper briefly summarizes the recent progress of atmospheric iron isotope geochemistry. We show that some of the major natural and anthropogenic PM sources have different iron isotopic compositions. A Bayesian isotopic mixing model MixSIAR was used to quantitatively re-evaluate the contributions of different sources to iron in both urban and marine aerosols based on iron isotopic data in the literature. The results highlight the value of stable iron isotope analyses as an effective tool in the source apportionment of atmospheric aerosols.

INTRODUCTION

In the last several decades, growing attention has been paid to the severe and persistent haze pollution, due to its negative effect on air quality[1], visibility[2], human health[3,4], and climate[5–7]. This environmental problem is mainly caused by anthropogenic emissions during rapid urbanization and industrialization, especially in developing countries[8,9]. Trace metals are important components of atmospheric particles, potentially contributing to chemical reactions in the atmosphere, and thus affect atmospheric pollution and climate. Once deposited on the surface ocean, trace metals such as iron, magnesium, and copper can serve as micronutrients to stimulate biological productivity[10]. Those trace metal-containing particles can be originated from natural sources including mineral dust, volcanic ash, wildfires, and anthropogenic sources including biomass burning, fossil fuel combustion, metallurgical production, and industrial emissions[11,12]. Once emitted into the atmosphere, these airborne particles can be transported and dispersed in air and finally removed by dry or wet deposition processes.

As one of the most abundant heavy metal elements in the earth's crust, iron is ubiquitous in both terrestrial and aquatic ecosystems, and is utilized in numerous physiological functions such as photosynthesis, biosynthesis, respiration, and fixation of nutrients[13]. The utilization of iron is thought to have an impact on the Earth system by affecting iron biogeochemical cycles[14,15], particularly for marine productivity. In remote marine ecosystems such as the subarctic, equatorial and Southern Oceans, which are called high-nutrient, low chlorophyll regions today, the phytoplankton community tends to be limited by iron[16]. Numerous in-situ iron fertilization experiments[15,17] confirmed that the increased iron supply would promote the fixation of macronutrients such as nitrogen and phosphorus, so as to increase primary productivity[18] and decrease carbon dioxide concentration[19]. Besides, iron is critical to the human body for Fe(II)-bearing haemoglobin in the

blood, Fe(III) ferritin in the liver and the kidneys, or serving as an enzyme cofactor[20]. However, it has been acknowledged that excessive biomedical exposure to iron oxide nanoparticles would induce cytotoxicity, developmental toxicity, neurotoxicity and gene damage[21]. Moreover, iron-bearing nanoparticles could cause cardiovascular and respiratory diseases and have been found in the human brain, serum and pleural effusion through ambient pollution exposure[22,23].

Various reservoirs such as margin sediments[24], rivers, groundwater, icebergs[25], sub-glacial runoff, and glacial flour dust[26] have been presented as external iron nutrient sources to the marine surface, but few of them are accessible to remote regions. Another important iron supply originates from magma and hydrothermal activities in the deep crust, but it is rapidly precipitated at depth and lost by subduction and has a limited impact on the surface ocean[27]. Differently, aeolian dust has long been considered an important iron supply to the surface ocean[28–30]. In modern systems, atmospheric particles are classified into two origins, namely natural and anthropogenic sources[31]. Natural sources include mineral dust, sea spray, wildfires, volcanoes, and biogenic emissions. For example, mineral dust dominantly originated from deserts, semi-arid regions, dry lake beds or channels where large amounts of alluvial sediment are accumulated as a result of annual scarce rainfall[32]. Sometimes, human-induced droughts and changes in land use can also increase mineral dust entrainment[33]. Natural sources are generally of large particle size and mostly settle back to the surface by gravity (dry deposition). By contrast, anthropogenic iron sources, including industrial manufacturing, traffic emissions, fossil fuel combustion and biomass burning (wood or crop residues burning by agricultural or household activities) are mainly produced by pyrogenic processes. Those primary aerosols, from either natural or anthropogenic sources, are generally ranging from 1 nm to 100 μm in diameter[31]. The residence time of those particles in the atmosphere ranges from

[1]Institute of Surface-Earth System Science, School of Earth System Science, Tianjin University, Tianjin, China. [2]Department of Atmospheric Sciences, School of Earth Sciences, Zhejiang University, Hangzhou, China. [3]School of Geography, Earth and Environment Sciences, University of Birmingham, Birmingham, UK. [4]Department of Environmental Sciences, Faculty of Meteorology, Environment and Arid Land Agriculture, King Abdulaziz University, Jeddah, Saudi Arabia. [5]These authors contributed equally: Yuantao Wang, Libin Wu. ✉email: fupingqing@tju.edu.cn

hours to weeks, depending on the particles' properties and the removal effectiveness[34,35]. The particle sizes of anthropogenically sourced particles rarely exceed 2.5 μm[36]. An exception to this is brake wear particles of which about 50% by mass exceed 2.5 μm[37]. Fine particles are generally characterized by a longer lifetimes and are often transported for several hundred or even thousand kilometres beyond the continental shelf[38].

The spatiotemporal variations in iron fertilization from atmospheric deposition are dependent on total iron loadings as well as iron solubility. Iron solubility typically ranges from <0.1% to almost 80% in atmospheric aerosols, but <0.5% in primary soil dust[39]. Atmospheric particles are systematically removed by preferential deposition mechanisms, leaving the particles with larger surface-to-volume values that are more soluble[40]. However, a modelling study indicated that this process is not significant and cannot explain the large increase in observed iron solubility from source regions to the remote ocean[41]. The iron solubility in atmospheric particles can increase via mineralogical transformation[42], photochemical redox processes[43,44], acidification in wet aerosol[45–47], and organic complexation[43,48,49].

Previous studies have indicated the importance of dissolved (bioavailable) iron from mineral dust on a global scale[50]. However, the supply of pyrogenic-sourced iron particles to the surface oceans may have been underestimated[51–54]. The soluble iron deposition from anthropogenic sources has increased as a result of continuing human perturbation over the Anthropocene[55,56], with an estimation of from 0.05 to 0.07 Tg yr^{-1} in the preindustrial era to 0.11–0.12 Tg yr^{-1} in the present day[57]. Moreover, a number of field and modelling studies have suggested that iron in at least some of the anthropogenic and combustion processes has a higher fractional Fe solubility (bioavailability)[46,57–64]. This has been evidenced by direct observation of either high fractional soluble iron in polluted aerosols or enhanced iron solubility when associated with anthropogenic emissions[46,58,60,62,65]. Hence, pyrogenic iron sources may contribute a considerable amount of soluble iron in aerosols although pyrogenic iron is less abundant compared with natural dust iron[62,64,66–69].

Nevertheless, it is difficult to ascertain whether the soluble iron is directly attributed to the anthropogenic component, or has been enhanced by complex atmospheric processing[70,71] or climate change[72]. For example, a measurement of iron solubility of ice-core dust in the Last Glacial Maximum (26,000–21,000 years before the present) varied between 1% and 42%, indicating that high iron solubilities are not purely a result of the presence of anthropogenic iron[73]. Our knowledge of soluble iron flux is limited by a large uncertainty on source contributions due to the lack of observational constraints. More recently, Zhu et al. applied receptor modelling to apportion the sources of dissolved Fe in a megacity for the first time[74]. However, there is very limited information on the sources of dissolved and total iron in atmospheric aerosols, particularly in the remote atmosphere.

Stable isotopes of volatile elements referred to as 'traditional isotopes' (carbon, hydrogen, oxygen, nitrogen, and sulfur), are generally characterized by large isotope mass differences and thus can be detected with pronounced isotopic variations in environmental samples[75,76]. Thus, traditional stable isotopes (e.g., $\delta^{13}C$, $\delta^{15}N$, $\delta^{18}O$) have been successfully applied as tracers for apportioning potential sources of contaminants in various environmental studies[77], such as plant ecology[78], diet reconstruction[79,80] and air pollutants[81,82]. Specifically, they have shown great performance in distinguishing aerosol sources and formation processes in the atmosphere[82–85]. This relies on the fact that isotope fractionations vary in different physical and chemical processes, resulting in a diversity of isotopic compositions in different isotope reservoirs. Stable isotopes can be used as signatures in both processes and sources in the environmental systems[86,87]. Process tracking relies on the understanding and quantification that iron isotopic compositions are altered when affected by transformation processes, such as redox reactions[88,89], complexation[90], acid leaching[91], evaporation[92] and biological uptake[93]. Source tracing is based on stable isotope mass balance and multiple sources with different isotopic signatures contributing to a mixing reservoir. The relative contributions from involved endmembers to a sample can be quantified by mixing calculations[87]. That is

$$Y = \sum p_k \mu_k \qquad (1)$$

where Y stands for isotopic compositions of the mixture, which has k possible sources; μ_k describes the mean isotope value for source k (after considering the isotope fractionation), and p_k is the proportional contribution of source k to the total amount ($\Sigma p_k = 1$). Source tracing has been applied in several metal stable isotope systems both in mass-dependent fractionation (MDF) and mass-independent fractionation (MIF) signatures[94,95], showing the potential in discriminating endmembers involved in mixing sources.

While the precise analyses of traditional stable isotopes are available by gas-source spectrometers, further progress for heavier elements, especially metal stable isotopes, has been restricted due to a lack of methodological improvements for years. Owning to the advances in isotope analytical instruments, particularly the multi-collector inductively coupled plasma mass spectrometry (MC-ICP-MS) since the 2000s, high precision analyses for a wide range of heavy metal isotopes are accessible now[96,97]. Analytical improvements make it possible to distinguish subtle variations between anthropogenic and natural samples, which can be further utilized as 'fingerprint information' for deducing inorganic contaminant behaviour through environmental processes. A wide range of heavy metal stable isotopes such as zinc, mercury, silver, and potassium have shown extensive applications in various environmental media[98–101]. Specifically, non-traditional stable isotopes including lead and strontium[102–104], silicon[105,106], mercury[107–109], zinc, and copper[110], have been shown to be effective tracers in determining sources of airborne contaminants and further atmospheric processes.

Tracking the sources of atmospheric particles precisely is a prerequisite for air pollution control. To access the environmental risks and to provide solutions for environmental metal pollution, understanding the sources, speciation, transformation and bioavailability of heavy metals is essential. Source identification and quantification are regarded as important goals for future research on comprehensively understanding the nature of nutrient delivery to the open ocean. Here, we review recent progress in the application of iron isotopes in atmospheric particulate matter. We firstly provided information on the analytical procedures and isotopic compositions of endmember iron sources, and then review the applications of stable iron isotopes in source apportionment. Furthermore, future perspectives of iron isotopes are also discussed.

STABLE FE ISOTOPIC COMPOSITIONS AND ANALYTICAL TECHNOLOGY

Basic concepts of iron stable isotopes

In the last several decades, iron isotopes have been widely utilized in studies of geological processes including high-temperature geochemistry, crust-mantle evolution, magmatic differentiation, hydrothermal processes and cosmochemistry[111]. Scientists have performed many applications of iron isotopes as signatures in redox and biogeochemical cycles[112,113], river systems[114] and terrestrial ecosystems[115] such as paddy soil[116,117]. Considering the important role of iron in biological processes in the human body, the iron isotope has been applied as a reliable pathological signature and is becoming a powerful indicator in medical diagnosis[20,22,118,119].
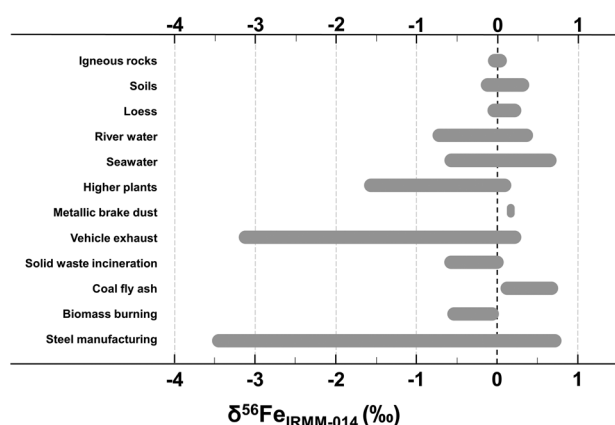
Fig. 1 **Iron isotopic variations (δ^{56}Fe, by reference to the IRMM-014 standard, shown as shadow bar) of natural and anthropogenic (pyrogenic) aerosol sources.** Natural sources include igneous rocks[125], soils[148,162], loess[163,164], river water[114,124], sea water[52,134,165], and higher plants[138]. Anthropogenic (pyrogenic) sources include metallic brake dust[143], vehicle exhaust[141], solid waste incineration[141,146], coal fly ash[128,146], biomass burning[140], and steel manufacturing[142,147].

Natural variations in non-traditional stable isotopes are generally very small, and hence are commonly reported as delta notation (δ) in unit of per mil (‰) with the ratio relative to an international standard. Iron has four stable isotopes, ^{54}Fe, ^{56}Fe, ^{57}Fe, and ^{58}Fe, with natural abundances of 5.84, 91.76, 2.12, and 0.28 atom %, respectively. Most studies have focused on the two most abundant isotopes, and reported isotopic compositions as δ^{56}Fe, with a deviation of ^{56}Fe/^{54}Fe ratio relative to geological standards. Some studies have also reported ^{57}Fe/^{54}Fe as δ^{57}Fe, but seldom reported δ^{58}Fe because ^{58}Fe is a scarce isotope. Isotopic variations are mostly reported relative to the IRMM-014 standard, although some geologists use average igneous rocks as the standard to define deviations (i.e., average δ^{56}Fe value of 15 terrestrial igneous rocks and 5 high-Ti lunar basalts, δ^{56}Fe$_{IRMM-014}$ = δ^{56}Fe$_{igneous\ rocks}$ + 0.09‰)[120]. Here, we will consider only δ^{56}Fe, and discuss iron isotopes relative to the IRMM-014 standard as follows:

$$\delta^{56/54}Fe(‰) = \left[\left(^{56}Fe/^{54}Fe \right)_{sample} / \left(^{56}Fe/^{54}Fe \right)_{IRMM-014} - 1 \right] * 1000$$

(2)

For those δ^{57}Fe ratios reported, data have been converted to equivalent δ^{56}Fe by assuming δ^{56}Fe ≈ 0.66 × δ^{57}Fe based on the mass-dependent fractionation relationship[121].

Analysis of iron isotopes

A careful chemical purification process is essential for accurate isotope analysis. Nowadays, mature pre-treatment methods for iron isotopes have been established, but mainly focusing on rocks and solid samples. Beard et al. reported the first value of iron isotopic compositions of airborne particulate matter[122]. Here, we summarize the basic approach for pre-treatment protocols including acid digestion and ion exchange chromatography.

The separation and purification usually start with acid digestion with mixed acids in a closed perfluoroalkoxy alkanes (PFA) vial with all equipment cleaned before usage. Firstly, approximately 1/40–1/20 (3–6 cm^2) of a filter is decomposed and transferred into a Teflon beaker to be digested by acids (the acid compositions depend on the properties of the samples). Secondly, the solution is evaporated nearly to dryness at 120 °C. In order to make sure that insoluble components are solubilised, and the Fe is in a ferric state, the solution is usually cycled through several digestion and

evaporation procedures. After that, the solution is taken up in acid for passages on the chromatographic column and then followed by analytical measurements. See Supplementary Note 1 for methods of ion exchange chromatography and instrumentation.

IRON ISOTOPIC COMPOSITION OF ATMOSPHERIC IRON SOURCES

Natural sources

Natural sources including volcanic ash, terrestrial dust, sea spray, and wild biomass burning can produce a large amount of atmospheric particulate matter, contributing to a natural background of iron-containing aerosols. In this section, we summarize the reported δ^{56}Fe ratios of natural iron repositories (Fig. 1, see Supplementary Table 1 for details).

Volcanic ash and terrestrial dust. There has been no report on iron isotopes of volcanic ash. Some volcanic rocks are characterized by isotope ratios ranging from −0.24‰ to 0.3‰[123,124], and hence it is possible that volcanic emissions have comparative or lower δ^{56}Fe ratios than that of the basalt or rhyolite. A number of studies revealed that iron isotopic compositions of terrestrial components such as sediments, topsoil, loess, and desert dust are nearly identical to those of the igneous rocks, implying a relatively constant isotope characteristic of detrital materials on the earth's surface under modern oxidation conditions. Beard et al.[125] investigated iron isotopic compositions of 46 igneous rocks, showing an average isotope value of 0.09 ± 0.10‰ (2 SD) from the different geological background, which is almost identical to the continental crust (0.07 ± 0.03‰, 2SD, converted to equivalent δ^{56}Fe$_{IRMM014}$) reported by Poitrasson[126]. On a global scale, aeolian dust is measured with a near-crustal endmember value of 0.09 ± 0.10‰ (2 SD). This is constrained by isotope ratios of aerosols (0.08 ± 0.08‰, 1SD) from the pioneering work of Beard et al.[122]. Marine aerosols under the influence of Saharan flux showed similar isotope ratios, 0.04 ± 0.05‰ (1SD) in Barbados[127] and 0.08–0.10‰ in Bermuda[128].

Sea spray. Sea spray aerosol (SSA) is generated from the ocean surface, with particle sizes ranging from <10 nm to several millimeters[129]. The annual global production of SSA is estimated to be 10^{13} kg, with ~32% from the Northern Hemisphere[130]. Additionally, airborne volcanic ash emitted along the Pacific Rim and from hot spots is a potentially underestimated iron source to the atmosphere[131]. It fertilizes the ocean and contributes to large phytoplankton blooms[132,133]. Surface seawater is generally found with δ^{56}Fe ratios for dissolved Fe of up to 0.73‰ in the North Atlantic[134]. This can be explained by the influence of aerosol deposition from the Saharan dust plume[134] and the preferential biological uptake of lighter Fe[135]. However, it was revealed that δ^{56}Fe ratios for dissolved Fe can be as low as −0.65‰ in the North Pacific Ocean, where the anthropogenic deposition may play a vital role in isotopic alteration of the surface seawater. However, no δ^{56}Fe data are available concerned directly with SSA. Further studies are necessary to clarify these findings.

Natural biomass burning. There are various biomass burning types, such as wild (forest, savanna, grassland) fires, wood or straw combustion as fuels, and agricultural crop residue burning[136,137]. Here, we mainly focus on natural processes. In most cases, biomass burning is a kind of point source that can increase atmospheric iron concentrations on a regional scale but has been considered an important bioavailable iron source to the oceans owing to its high iron solubility[63]. Some higher plants (including dicots, non-grass monocots and grass species) may originally have δ^{56}Fe values from −1.64‰ to 0.17‰[138], and biomass burning ash is hence expected with a relatively low δ^{56}Fe signature. For example, Mead et al.[128] suggested that biomass burning plumes

were responsible for negative $\delta^{56}Fe$ ratios ($\leq -0.5‰$) collected in fine particles from Bermuda marine aerosols, although there was no direct evidence. However, the $\delta^{56}Fe$ values of burning plumes are not purely indicative of biomass burning aerosols because soil-derived particles have been observed in outfield burning events[48,139]. The existence of soil components can be attributed to the suspension of dust that had been deposited onto the vegetation, or the uplift of the burned soil surface driven by turbulence created by the fire[35]. Soil dust can largely influence burning emissions due to its higher content of Fe than that in plants. The isotopic signals from biomass burning ash are low and hence are likely to be obscured by a large amount of soil suspension. Furthermore, the combustion output of biomass burning largely depends on the surface circumstances, such as biomass species, the density of vegetation and soil properties. Therefore, the isotope characteristics of wild biomass burning aerosols can differ among various plants, soil components and burning conditions.

Anthropogenic sources

Iron isotopes can be used as fingerprints for anthropogenic sources (combustion and industrial activities) because iron can be highly fractionated during pyrogenic processes. However, data on $\delta^{56}Fe$ of those emissions remain limited. Pyrogenic iron sources include (1) biomass burning events (In this section, we mainly focus on human-induced processes), (2) road traffic emissions such as automobile exhaust and abrasion of metallic brake pads, (3) municipal solid waste incinerator (MSWI) and coal fly ash, and (4) industrial activities such as metallurgical processes and other miscellaneous emissions.

Biomass burning events. A recent study provided the first insight into $\delta^{56}Fe$ values of a field reed burning event in Japan[140]. The results indicated that the $\delta^{56}Fe$ ratios of fine particles (0.39–0.69 μm) collected during the event were from $-0.61‰$ to $-0.36‰$, higher than those ($\delta^{56}Fe = -1.06 \pm 0.12‰$ and $\delta^{56}Fe = -1.26 \pm 0.13‰$, 2SD) before and after the event, thereby suggesting the influence of soil-derived Fe in burning plumes. A further experiment was conducted to reduce the soil suspension interference, indicating no clear iron fractionation signals during the open biomass burning event.

In the reed burning event, the combustion temperature was estimated to be approximately 300–500 °C[140], which is lower than those of anthropogenic combustion processes such as automobile exhaust and steel metallurgy[141,142]. Hence, it is unclear whether a sufficient amount of iron can be fractionated during the biomass burning processes. However, the amount of fractionated iron isotopes is not only impacted by combustion temperature, but also by other factors, such as vapour pressure, iron species, and other coexistent elements[92]. Both laboratory experiments and field observations on different burning circumstances are worth the effort to clarify whether isotope fractionation of Fe in a burning event is distinct enough to be observed, so as to verify the values of iron isotopes as biomass burning aerosol tracers.

Road traffic emissions. It has been shown that iron can be highly fractionated during the combustion of gasoline or light diesel oil[141]. Specifically, isotopically light $\delta^{56}Fe$ values of bulk aerosols (-3.2–$0.3‰$) were observed in a road tunnel at Hiroshima, Japan, which was lower than that of the local terrestrial dust ($0.18 \pm 0.22‰$, 2SD) or commercial gasoline ($0.28 \pm 0.13‰$, 2SD). The isotope values of aerosols in the tunnel exhibited a clear size dependence. For example, 91% of Fe was found in coarse particles larger than 1.1 μm with $\delta^{56}Fe$ values from $-0.1‰$ to $0.3‰$. Fine particles <1.1 μm originated mainly from vehicle exhaust and were characterized with $\delta^{56}Fe$ values as low as $-3.2‰$. Moreover, Majestic et al.[143] found that $\delta^{56}Fe$ ratios of both fine and coarse

particles (0.12–0.22‰) collected in a parking garage were most likely attributed to the abrasion of metallic brake pads (average = 0.18‰), further indicating that the extremely low $\delta^{56}Fe$ ratios observed in the road tunnel can be attributed to the combustion of fossil fuel.

Incinerator use. Previous studies have investigated chemical and mineralogical characterization of MSWI residues[144,145], showing that metals with low volatility such as iron mainly remain in the bottom ashes during incineration. Small iron particles are formed as (hydr)oxides, and carried over by flue gas through the furnace. MSWI residues were reported with comparable $\delta^{56}Fe$ values, ranging from $-0.10‰$ to $0.10‰$[141,146]. However, distinguishable isotopic variation was detected between bottom ash ($\delta^{56}Fe = -0.34 \pm 0.14‰$, 2SD) and fly ash ($\delta^{56}Fe = -1.97 \pm 0.18‰$, 2SD) collected at the incinerator if extracted by HCl solutions[141]. The results of Kurisu et al.[141] indicated that only a small amount of iron was evaporated during incineration, and finally incorporated into the total suspended particles (TSP, $\delta^{56}Fe = -0.66 \pm 0.09‰$, 2SD). The iron isotopic compositions of coal fly ash were from 0.05‰ to 0.75‰[128,146], implying that not all anthropogenic (pyrogenic) processes may release light $\delta^{56}Fe$ values.

Industrial manufacturing. Flament et al. investigated iron isotopic compositions of TSP from a steel plant in France, Europe[147]. The isotope ratios were found slightly decreased from sintering (a mixing state at high temperature, consisting of ore, coke and additives, $0.53‰ \leq \delta^{56}Fe \leq 0.80‰$) to steelworks emissions ($\delta^{56}Fe = 0.08 \pm 0.24‰$, 1SD). However, there was no significant iron isotope fractionation occurring during metallurgical processes, because $\delta^{56}Fe$ ratios of raw ore materials ($-0.16‰$ to $1.19‰$) were found similar to steelworks emissions (0.08–0.80‰). In contrast, according to a recent study, the temperature (1000–2000 °C) during metallurgical processes was expected to be high enough for isotope fractionation[142]. Fine particles (0.39–1.3 μm) were found to yield lower $\delta^{56}Fe$ values ($-3.53‰$ to $-0.37‰$) during evaporation, quite different from those of the coarse particles (≥ 1.3 μm, $-0.42‰$ to $0.33‰$) and ore components ($\delta^{56}Fe = -0.27 \pm 0.13‰$, 2SD). Given that $\delta^{56}Fe$ can be calculated by a combination of two end-members with different iron isotope values, Kurisu et al. suggested a value from $-4.7‰$ (by calculation) to $-3.9‰$ (by observation) as the isotopic signature for evaporated iron from a steel plant[142], which is the lowest $\delta^{56}Fe$ from anthropogenic sources that was ever estimated[140–142,148]. The difference in $\delta^{56}Fe$ values for steel plant emissions in the aforementioned studies is likely attributed to the manufacturing technologies and diverse ore materials across different regions. One recent case study on steelworks has also shown that much of the emitted PM arises from the transfer of ores and dust from site roads[149]. More investigations are needed to verify the use of iron isotopes as indicators for metalworking emissions.

APPLICATION OF IRON ISOTOPES TO TRACE SOURCES IN AEROSOLS

Stable isotopic compositions of aerosol iron have been investigated on various spatial and temporal scales, but most of them were studied for marine aerosols in the Northern Hemisphere (Fig. 2 and Supplementary Table 2). If iron isotopic compositions differ between pyrogenic (anthropogenic and combustion) and natural sources, stable isotopes are potential tracers to constrain source contributions and are used as a tool in apportioning atmospheric iron.
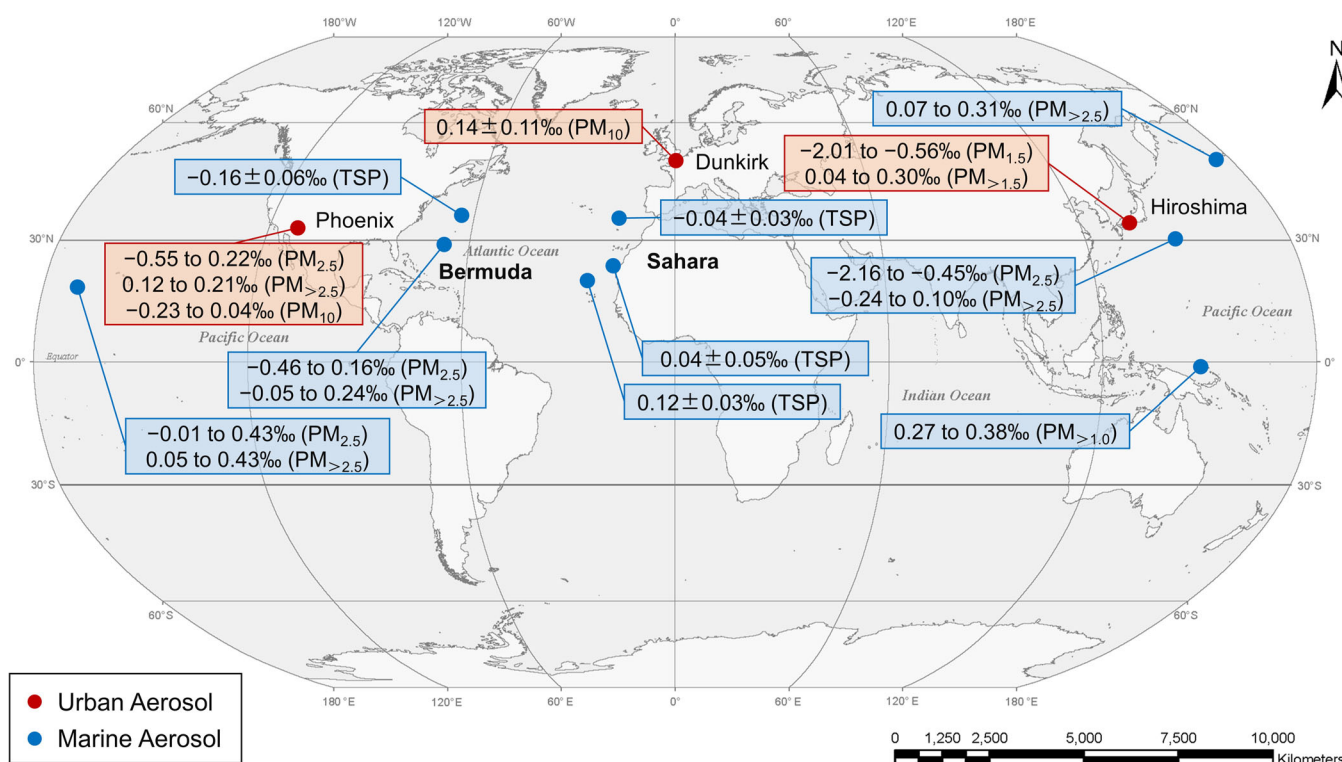
Fig. 2 Iron isotopic compositions (δ^{56}Fe for total Fe) of urban and marine aerosols in the literature. Urban aerosol studies include Phoenix, America[150], Dunkirk, France[147], and Hiroshima, Japan[148]. Marine aerosol studies include Northwest Pacific[148,152], Western Equatorial Pacific[155], and North Atlantic[71,127,128]. For the average δ^{56}Fe data on the graph, measurement accuracy is shown as 1 standard deviation (1 SD).

Size-segregated isotope ratios as an indicator of iron sources

In early studies, little or no isotopic variations were detected in terrestrial and marine aerosols[122,127,147,150]. This is because atmospheric aerosols can be affected by a variety of iron sources from both natural and anthropogenic processes, of which the isotopic fingerprints in variable size fractions can sometimes be overlapped and mixed. However, in view of the fact that anthropogenic activities are likely to yield finer particles with lower δ^{56}Fe values than natural sources, it is possible to distinguish anthropogenic sourced iron with light isotopic signals from the ubiquitous soil dust background. Thus, isotopic fingerprints can be partially separated from each other by using size-segregated aerosol sampling methods.

Urban aerosols. The first iron isotopic assessment of size-segregated suburban aerosols was conducted near Phoenix, USA for atmospheric particles with an aerodynamic diameter $\leq 2.5\ \mu m$ ($PM_{2.5}$) and 10 μm (PM_{10})[150]. The δ^{56}Fe ratios in $PM_{2.5}$ ($-0.55‰$ to $-0.22‰$) were substantially lower than those in PM_{10} ($-0.23‰$ to $0.04‰$). Further evidence identified the spatiotemporal source patterns in fine particles, while coarse particles mainly originated from crustal dust. Another size-segregated iron isotopic measurement of urban aerosols was performed in Hiroshima, a coastal city in Japan[148]. Aerosols were separated into seven size fractions, providing a better insight into size distributions of iron isotopic compositions. The iron isotope ratios were measured as low as $-1.59‰$ in particles in the size range of 0.39–0.69 μm collected in spring, while summer aerosols showed lower ratios of $-2.01‰$ in the same size range. Assuming that the samples were numerically divided into two fractions of particles, i.e., finer and coarser than 1.5 μm, the isotope values of fine particles showed a very negative value of $-2.01‰$ to $-0.57‰$. By contrast, in coarse particles, the isotope ratios ranged from $0.04 \pm 0.07‰$ (1SD) to $0.30 \pm 0.07‰$ (1SD), which are almost identical to the crustal sources. These two

size-segregated isotopic measurements demonstrated a different source distribution of atmospheric iron between fine and coarse particles, implying the potential of using δ^{56}Fe values as signatures in tracing multiple iron sources. Noteworthily, a recent study reported δ^{56}Fe values of airborne Fe-bearing magnetic particulate matter (MPs, a frequent component of $PM_{2.5}$, is not only formed naturally but also can be released from human activities) in $PM_{2.5}$ and $PM_{>2.5}$ during sandstorm episodes in Beijing, China[151]. The isotopic compositions of Fe in MPs were 0.10–0.19‰ in $PM_{>2.5}$ collected during a sandstorm, which was identical to the natural crustal composition. By contrast, the δ^{56}Fe ratios of MPs in $PM_{2.5}$ were $-0.49‰$ to $-0.10‰$ and $-0.70‰$ to $-0.44‰$ in the sandstorm and non-sandstorm periods, respectively. The heterogeneous δ^{56}Fe values of MPs in $PM_{2.5}$ were most likely attributable to anthropogenic emissions with light Fe isotopic compositions, even during the sandstorm period[151].

Marine aerosols. Marine aerosols are characterized by a mixture of both natural and anthropogenic emissions from long-range transport. Several observations of iron isotopic compositions have been conducted in the North Atlantic, an ideal place for studying iron aerosol sources. During most of the time in summer, a large influx of crustal dust (mostly from North Africa) is transported to the North Atlantic, while for the rest of the time, various non-crustal sources such as biomass burning and oil fly ash might contribute more[71,128]. A recent study of TSP collected from the North Atlantic Ocean has described an iron isotopic shift along the cruise[71]. The aerosol samples were separated into three groups based on cruises that were mostly influenced by air masses from Europe, Sahara, or North America. The results indicated that aerosols mostly impacted by the Saharan plume were identified with an average δ^{56}Fe ratio of $0.12 \pm 0.03‰$ (1SD). In European and North American air masses-dominated aerosols, however, the δ^{56}Fe ratios were determined to be $-0.04 \pm 0.03‰$ (1SD) and

−0.16 ± 0.06‰ (1SD), respectively. This can be explained by the fact that samples collected close to North Africa were characterized by a higher amount of dust, thus displaying a near-crustal isotopic signature. The isotopically negative signature in non-Saharan-dominated samples is associated with anthropogenic emissions. Another year-round observation in Bermuda evaluated iron isotope characteristics in size-segregated samples, providing further evidence of non-crustal iron sources in marine aerosols[128]. Fifty-three coarse particle (>2.5 μm) samples collected in Bermuda were found to be isotopically comparable, with an average value of 0.10 ± 0.11‰ (2SD). While in the corresponding 52 fine particles (≤2.5 μm) samples, iron isotope ratios showed a seasonal pattern, with a wide variation from −0.46‰ to 0.16‰. The negative δ^{56}Fe ratios in fine particles presumably indicate an important non-crustal iron source, most likely from biomass burning or other anthropogenic emissions via long-distance transport offshore from North America.

In some cases, marine aerosols were characterized by an isotopic background of natural sources. However, many observations have demonstrated the impact of anthropogenic disturbance on the remote ocean, e.g., in the Northwest Pacific[52,152]. This has been evidenced by the observation of an extremely low δ^{56}Fe ratio of −0.65‰ in surface seawater from the North Pacific Ocean, which is ascribed to a preferential long-range transport of anthropogenic emissions with finer particle sizes than the natural dust. In particular, marine aerosols near East Asia are characterized by more human-related emissions than crustal materials. For example, marine aerosols near the Japanese coast exhibited δ^{56}Fe ratios from −2.16‰ to −0.45‰ in $PM_{2.5}$ samples, lower than those of the $PM_{>2.5}$ samples from −0.24‰ to 0.10‰[148,152]. These are the lightest δ^{56}Fe values that were ever detected for total Fe collected in marine aerosols.

Dissolved iron isotope ratios as an indicator of anthropogenic emissions

The aforementioned observations are indicative of the presence of isotopically negative δ^{56}Fe signatures in both urban and marine aerosols, showing that iron isotopes can be helpful to distinguish anthropogenic emissions from natural components. However, isotopically negative signatures of anthropogenic iron can sometimes be masked in isotope ratio analysis, making it difficult for source identification even via size-segregated measurements. One feasible solution to this barrier is to extract dissolved iron by means of water (also referred to as rainwater or seawater) dissolution. Previous studies have indicated that combustion iron is more prone to be preferentially dissolved[46,57–63]. Hence, pyrogenic and combustion-sourced iron with low δ^{56}Fe signals can be amplified due to the preferential dissolution[152].

For example, the δ^{56}Fe values for dissolved Fe measured in size-segregated urban aerosol samples from Hiroshima showed an isotopic variation from −2.58‰ to 0.47‰ in March and from −3.91‰ to −0.24‰ in August[148]. These isotope ratios obtained via extraction by simulated rainwater were lower than those of the total phase characterized with δ^{56}Fe ratios from −1.59‰ to 0.23‰ and from −2.01‰ to 0.30‰ in March and August, respectively. It is notable that the δ^{56}Fe value for dissolved Fe of −3.91‰ observed in the 0.39 μm fraction during August is the lightest isotopic signature that was ever found in aerosols. Isotope ratios of dissolved iron from marine aerosols were also reported in the North Atlantic Ocean[71] and the Northwest Pacific[152]. Compared with the δ^{56}Fe value for total Fe of North American and European air masses collected in the North Atlantic mentioned above (mean δ^{56}Fe = −0.12 ± 0.06‰, 1SD), the δ^{56}Fe value for water-dissolved Fe was −0.80‰ to −1.60‰ (mean −0.91‰), showing even lighter ratios of −1.45‰ in seawater-dissolved phases. For marine aerosols in the Northwest Pacific, which were collected near the Japanese coast and impacted by

many air masses from East Asia, dissolved Fe was showing lower δ^{56}Fe ratios of −0.27‰ ($PM_{2.5}$), −1.14‰ ($PM_{>2.5}$) and −2.23‰ ($PM_{>2.5}$) than those of the total Fe (0.10‰, −0.47‰ and −0.45‰, respectively). These lower δ^{56}Fe values in dissolved Fe fractions are mostly attributed to the preferential dissolution of anthropogenic components with low isotopic features[152], giving further evidence of low δ^{56}Fe signals of soluble Fe as an indicator of anthropogenic and combustion emissions.

Possible reasons for remarkably high and low isotope ratios in aerosols

In the aforementioned studies, negative δ^{56}Fe signatures from marine aerosols were likely to be anthropogenically originated from the land, or from local pollution such as shipboard emission plumes[153,154]. However, previous observations of remarkably low δ^{56}Fe ratios of total Fe in fine particles observed in the North Atlantic[128] (as low as −0.46‰) and Northwest Pacific[152] (as low as −2.16‰) implied that isotope ratios in the remote ocean were likely to be associated with secondary fractionation during the atmospheric transport because no materials with low δ^{56}Fe ratios were found as potential contributory factors.

Furthermore, remarkably high ratios were observed in the Northwest Pacific[152]. It was found that marine aerosols impacted by eastern and northern Pacific air masses were showing higher δ^{56}Fe ratios than the typical crustal values, even reaching as high as 0.43‰ in both fine ($PM_{2.5}$) and coarse ($PM_{>2.5}$) particles[152]. Heavier-than-crustal δ^{56}Fe ratios ($PM_{>1}$, from 0.27‰ to 0.38‰, 2 SD) were also observed in marine aerosols from the western equatorial Pacific, where anthropogenic pollution is really limited[152,155]. As far as we learn, these isotopic signals are not likely to be originated from mineral dust or anthropogenic emissions. Kurisu et al. have discussed possible explanations for such high δ^{56}Fe values[152], which could be attributed to (i) the presence of SSA or (ii) the change in δ^{56}Fe ratios during the transport of dust aerosols. It is likely that SSA could be responsible for the increase of δ^{56}Fe ratios in remote ocean aerosols as we discuss in Sect. 3.1.

Overall, isotopic compositions of aerosols not only depend on primary signals of iron sources but also are related to secondary isotope fractionations. This may happen during photochemical reactions, acidification process or even ligand complexation of the particles during long-range atmospheric transport. However, detailed mechanisms controlling the isotope fractionation of iron in the atmosphere are far from being fully understood.

EVALUATING CONTRIBUTIONS OF IRON SOURCES USING ISOTOPE MIXING MODEL MIXSIAR

Stable iron isotopes have been applied in calculation[134,156] and modelling[71] studies in both surface ocean and atmosphere environments to estimate contributions of different iron sources. Kurisu et al.[132] recently estimated the contributions from natural and combustion Fe to size-segregated marine aerosols by using a two-endmember mixing equation and an atmospheric chemical transport model. However, studies on quantitative source apportionment of iron in both urban and marine aerosols are limited. Here we conduct a mass balance calculation based on previously reported data of selected δ^{56}Fe endmembers of iron sources and aerosol samples (Supplementary Table 3). By using the Bayesian–Markov chain Monte Carlo (MCMC) simulation method MixSIAR, we re-evaluate the contributions of major iron sources for urban and marine atmospheres.

Source apportionment methods

Isotope mixing model. The MixSIAR model is a Bayesian Markov chain Monte Carlo (MCMC) simulation method, established under a Bayesian statistical framework and implemented as an open-

source R package. More details about the model have been reported in the previous studies[157,158]. The Bayesian mixing model was initially created in the studies of ecology and biology, e.g., food-web analysis[159], to assess the contribution of a predator's diet from different prey. Recently, it has been successfully applied to quantify the proportional contributions from different sources to atmospheric pollutants[81,82].

By using stable isotopes, the Bayesian model can help to determine the probability distributions of sources in a mixture and the contribution uncertainties of multiple sources. In each run of the MixSIAR model, respective mean and standard deviation parameters of anthropogenic and natural $\delta^{56}Fe$ endmembers, corresponding with every $\delta^{56}Fe$ value of fine or coarse fraction aerosol samples, were loaded. The model will generate a likelihood of iron source attribution and scaled posterior density based on the provided data. See Supplementary Note 2 for more details of the model operation procedures.

Determination of iron sources. As indicated by HYSPLIT backward trajectories and enrichment factors (EFs) analysis, aerosols in Hiroshima were greatly impacted by aeolian dust from Asia[148]. The existence of a large amount of Na^+ indicated SSA in a coastal city. The concentration of metal elements (Ni, Zn, and Pb) in both the March and August samples suggested a large contribution of anthropogenic activities such as fossil fuel combustion or metal production to urban aerosols. However, although previous studies have demonstrated large contributions from biomass burning or volcanic ash to atmospheric iron, they are not included in our calculations since there was neither an ambient burning event nor a large-scale volcanic eruption during the observation period. To be brief, terrestrial dust and sea spray were considered dominant natural sources in all calculations. In urban aerosols, we adopt fossil fuel combustion and steel plant emissions as major anthropogenic sources. By contrast in marine aerosols, in light of a continuous background delivery of offshore anthropogenic-derived flux, we directly choose a representative end member of fossil fuel combustion as an isotopic signature for evaporated iron sources.

Natural and anthropogenic $\delta^{56}Fe$ endmembers. We choose the crustal $\delta^{56}Fe$ value of $0.09 \pm 0.10‰$ (2SD) for typical dust endmember in all marine calculations. This value can be supported by the identical observations on $\delta^{56}Fe$ values of coarse mode particles in the North Atlantic (average 0.04–0.12‰)[71,127,128] and Hiroshima (0.04–0.30‰)[148]. It should be pointed out that, according to studies by Kurisu et al., the isotopic signature of local weathered granite ($\delta^{56}Fe = 0.18 \pm 0.22‰$, 2SD) is considered a better choice and hence applied as aeolian dust endmember in the calculations of Hiroshima[141,148]. The $\delta^{56}Fe$ values of SSA are directly substituted by the mean of $\delta^{56}Fe$ values from ocean surface water. In specific, an average $\delta^{56}Fe$ value of $0.42 \pm 0.17‰$ (1SD) is applied in model calculations for marine aerosols in the North Atlantic, which is determined by isotopic data of 13 surface water (2 m) samples collected during the USGT North Atlantic cruises[134]. An average $\delta^{56}Fe = -0.25 \pm 0.26‰$ (1SD), determined by 9 North Pacific Ocean surface (10–15 m) samples taken along the latitudinal transect at 158°W from 25°N to 42°N[52], was applied in Hiroshima and Northwest Pacific aerosols (Supplementary Table 3).

It should be mentioned that the model results are closely related to the choice of anthropogenic end members involved in calculations. For example, Conway et al.[71] conducted a two-component isotope mixing calculation of atmospheric Fe by using an assumed anthropogenic endmember of $-1.6‰$. They showed that the dissolved Fe in marine aerosols is contributed 50–100% from anthropogenic sources and suggested an underestimation of the contribution from such sources in model results. Recent work carried out a similar study using an endmember from $-3.9‰$ to $-4.7‰$ as combustion Fe, showing that the proportion of

combustion Fe in marine aerosols reaches as high as 51% and 20% in fine and bulk particles, respectively[152]. One barrier to source apportionment in aerosols is that it is difficult to determine the evaporation fingerprints of anthropogenic emissions. This is because those fine particles collected from near-source environments also contain some natural dust. Hence, the anthropogenic endmembers are possibly lower than the observed $\delta^{56}Fe$ ratios collected in fine-mode particles. This has been suggested by a calculated $\delta^{56}Fe$ value of $-4.7‰$, rather than $-3.53‰$ observed in fine-mode aerosols, proposed as the representative $\delta^{56}Fe$ end-member of steel plant emissions[142]. However, the $\delta^{56}Fe$ values of anthropogenic emissions were rarely reported. Available data include $\delta^{56}Fe$ of automobile exhaust (from $-3.2‰$ to 0.3‰) in a road tunnel, and ambient outflow from a steel plant (from $-3.53‰$ to 0.33‰)[141,142], as mentioned in Section 3.2. In these near-source cases, we assume that no isotope fractionation was occurring from emissions to sampled aerosols. In our analysis, to reduce the uncertainty caused by the selection of $\delta^{56}Fe$ endmembers, we tentatively propose an endmember decided by ultra-fine particles from automobile exhaust ($-3.2‰$ to $-0.3‰$) as fossil fuel combustion[141], and a recommended evaporation $\delta^{56}Fe$ value from $-4.7‰$ to $-3.9‰$ as steel manufacturing[142] (Supplementary Table 3).

Model calculation results

For the case of urban aerosols in Hiroshima, see Supplementary Fig. 1 for posterior estimates of proportional contributions of iron sources. The results demonstrated a similar source distribution in urban aerosols between March and August (Fig. 3, Supplementary Table 4). Aeolian dust contributed slightly more in March (26.3% in $PM_{1.5}$ and 82.2% in $PM_{>1.5}$) than that in August (21.7% in $PM_{1.5}$ and 74.0% in $PM_{>1.5}$), which could be easily explained by the impact of Asian dust outbreaks during the spring. It should be noticed that the contribution of anthropogenic sources is quite different in fine and coarse particles ($PM_{1.5}$) in both seasons. Steel plant and fossil fuel combustion accounted together for 4.6–6.9% in $PM_{>1.5}$, but reached up to 46.7% in $PM_{1.5}$ in August samples.

For the case of marine aerosols, see Supplementary Fig. 2 for posterior estimates of proportional contributions of iron sources. In the North Atlantic (Fig. 3, Supplementary Table 5), aeolian dust had a remarkable impact, with a contribution of 53.5%, 46.5% and 42.4% in air masses from Sahara, Europe, and North America, respectively. Seaspray emissions and fossil fuel combustion contributed 36.2–38.9% and 7.9–21.4% in marine aerosols, respectively. Of most interest was the increasing anthropogenic (representative of fossil fuel combustion) contributions in the order of Saharan (7.9%), European (14.7%) and North American (21.4%) air masses, which implied a heterogeneity of anthropogenic disturbance in the North Atlantic atmosphere. In the Northwest Pacific (Fig. 3, Supplementary Table 5), the results of bulk particles indicated that terrestrial dust, sea spray emission, and fossil fuel combustion were 28.7%, 47.9% and 23.5% in the source distribution, respectively. Specifically, fine particles ($PM_{2.5}$) were thought to include a large contribution from sea spray (38.1%) and anthropogenic emissions (50.4%). By contrast in coarse ($PM_{>2.5}$) particles, terrestrial dust was the dominant contribution reaching up to 75.7%, while anthropogenic emissions transported from East Asia only contributed 5.5%. Here, our calculation results were similar to one previous work using a two-endmember mixing model which suggested that the combustion Fe to total Fe in the Northwest Pacific was respectively estimated to be 50% and 6% in $PM_{2.5}$ and $PM_{>2.5}$[152].

In order to obtain a detailed insight into iron source apportionment in variable size fractions, we further calculated the size-segregated urban aerosol samples in Hiroshima. Posterior estimates of proportional contributions of iron sources can be
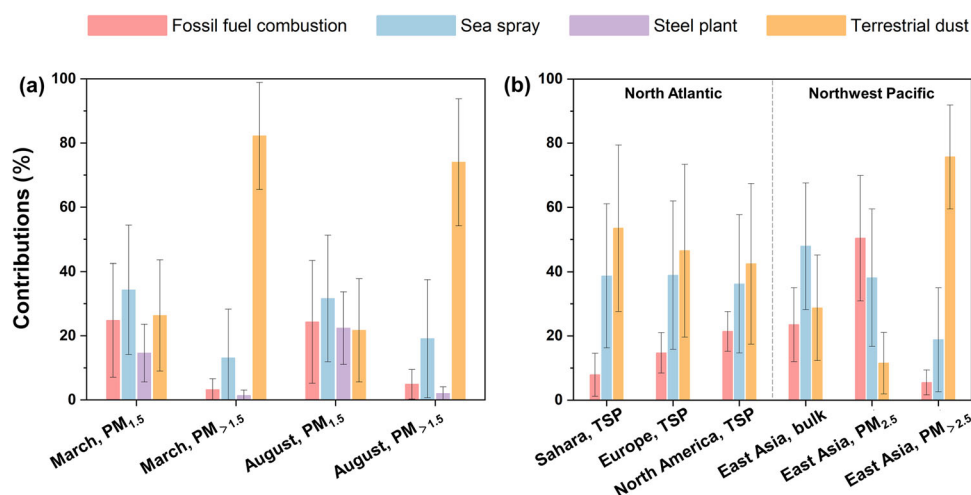
Fig. 3 Iron source apportionment results (mean ± standard deviation) based on model calculations with iron isotope ratios of different size particles from urban and marine aerosols. Source apportionment results in **a** Hiroshima, **b** North Atlantic and Northwest Pacific. Marine aerosols are classified according to the dominant impact of air masses[71,152]. For the Northwest Pacific, bulk particles are referred to coarse (PM>2.5) + fine (PM2.5) fractions. Original data of Hiroshima, Northwest Pacific and North Atlantic is from Kurisu et al.[148,152]. and Conway et al.[71], respectively. See Supplementary Tables 4–6 for model calculation uncertainties of the results.

found in Supplementary Figs. 3 and 4 for March and August samples, respectively. The results indicated a distinct size-segregated pattern of iron source distributions in both sampling periods (Fig. 4, Supplementary Table 6). Specifically, anthropogenic sources of the steel plant and fossil fuel combustion reached a peak in the <1.3 μm size mode, contributing from 26% to 57% in March and 24–64% in August, respectively. It is well acknowledged that fractionated iron is more likely condensed into tiny particles, and eventually incorporated into the fly ash. By contrast in the >1.3 μm size mode, terrestrial dust was the dominant iron source (~60%), while anthropogenic emissions only contributed <17%.

According to our model calculations, iron source distributions in aerosols were distinctly different in Hiroshima, the Northwest Pacific and the North Atlantic. The results indicated that East Asian air masses were much perturbed by anthropogenic emissions[148], while the North Atlantic aerosols were dominant by natural sources such as aeolian dust and sea spray[71]. We also showed that anthropogenic iron sources were more likely to condense in fine particles, while natural sources contributed largely to the coarse mode.

SUMMARY AND FUTURE PERSPECTIVES

In this review paper, we briefly summarize the recent progress of atmospheric iron isotope geochemistry, including the isotope characteristics of major sources of atmospheric iron, with emphasis on its application in the source apportionment of atmospheric pollutants (Fig. 5). Iron isotopes were used as source tracers to apportion atmospheric iron by means of a Bayesian stable isotope mixing model MixSIAR combined with reported isotopic data. We re-evaluate the contributions of natural and anthropogenic iron sources to urban and marine aerosols according to the previous literature, putting forward a source apportionment in a size-segregated aerosol. Our results demonstrate the potential usage of iron isotopes for both qualitative identification and quantitative calculation. However, the source tracing in natural systems is often complicated due to several barriers, for instance: (1) multiple sources of atmospheric particles, (2) unknown or overlapping isotopic signatures of mixing endmembers, (3) changes in isotopic signatures during atmospheric transport, and (4) uncertainties in mathematical models. Future work should consider:

1. High-quality pre-treatment of aerosol samples is required for the precise measurements of heavy metal stable isotopes. Hence, avoidance of contamination is a key requirement. Specifically, effective analytical performance would not be achieved without sufficient sample mass, because metal elements are primarily generated from the Earth's surface with a relatively low concentration in the atmosphere. Currently, chemical pre-treatment protocols for iron isotope analysis were initially established for measuring geological samples (i.e., rocks,). More effort should be made to develop a more timesaving, and suitable pre-treatment method for aerosol samples.

2. In order to avoid misinterpretation of isotopic fingerprints, a comprehensive and in-depth investigation of fractionation mechanisms during atmospheric processes is required. The isotopic fingerprints of iron sources are not only characterized by origins but also related to physicochemical changes that potentially occur during transport. Thus, the identification signals can be blurred and ultimately can mislead the source interpretation. However, the specific mechanisms of these processes are complex in the environment and are poorly known. Although it is not easy to draw a clear conclusion at present, clarifying the mechanisms by which iron isotopic compositions are changed can help to understand atmospheric transport processes and identify sources of iron. To address these issues, more effort should be made to evaluate the impact of atmospheric processes (e.g., photochemical reactions and acidifications) on isotope fractionation during the transport of Fe.

3. Isotope measurements of a wider range of iron sources are needed to establish a comprehensive database for isotope characteristics. A better understanding of the source apportionment can be limited by a lack of isotopic signatures and recognition of potential sources. As a matter of fact, the isotopic signals of iron sources are heterogeneous and are not sufficiently covered by a typical isotope value most of the time. Some potential sources share a similar range of isotope values, and thus cannot be distinguished in the source apportionment. When the isotopic signals of a single-isotope are overlapped, the use of multi-isotope analyses, either from the same element[106] or from others[160], is a potential solution to such obstacles in the future.
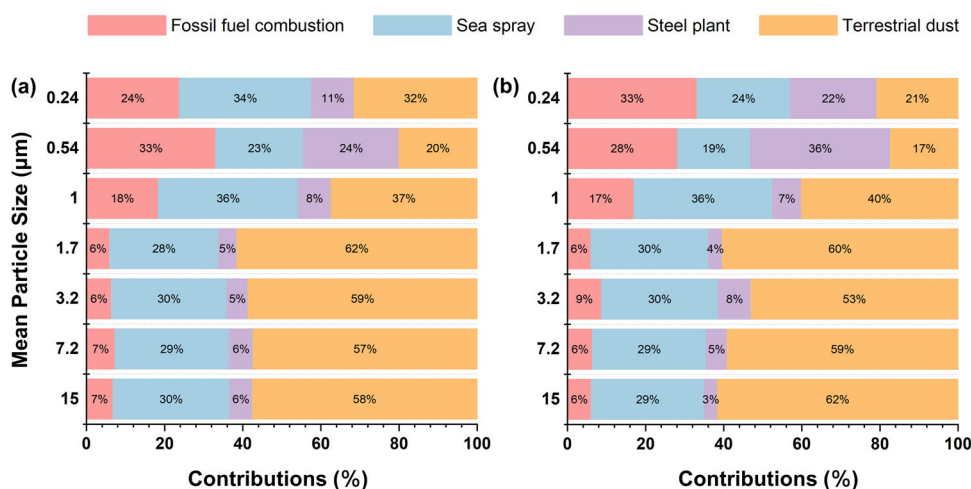
Fig. 4   Iron source apportionment results based on model calculations with iron isotope ratios of size-segregated aerosols in Hiroshima, Japan. Stacked bars show the results of **a** March and **b** August aerosol samples, respectively. Original data of Hiroshima size-segregated aerosol samples are from Kurisu et al.[148].
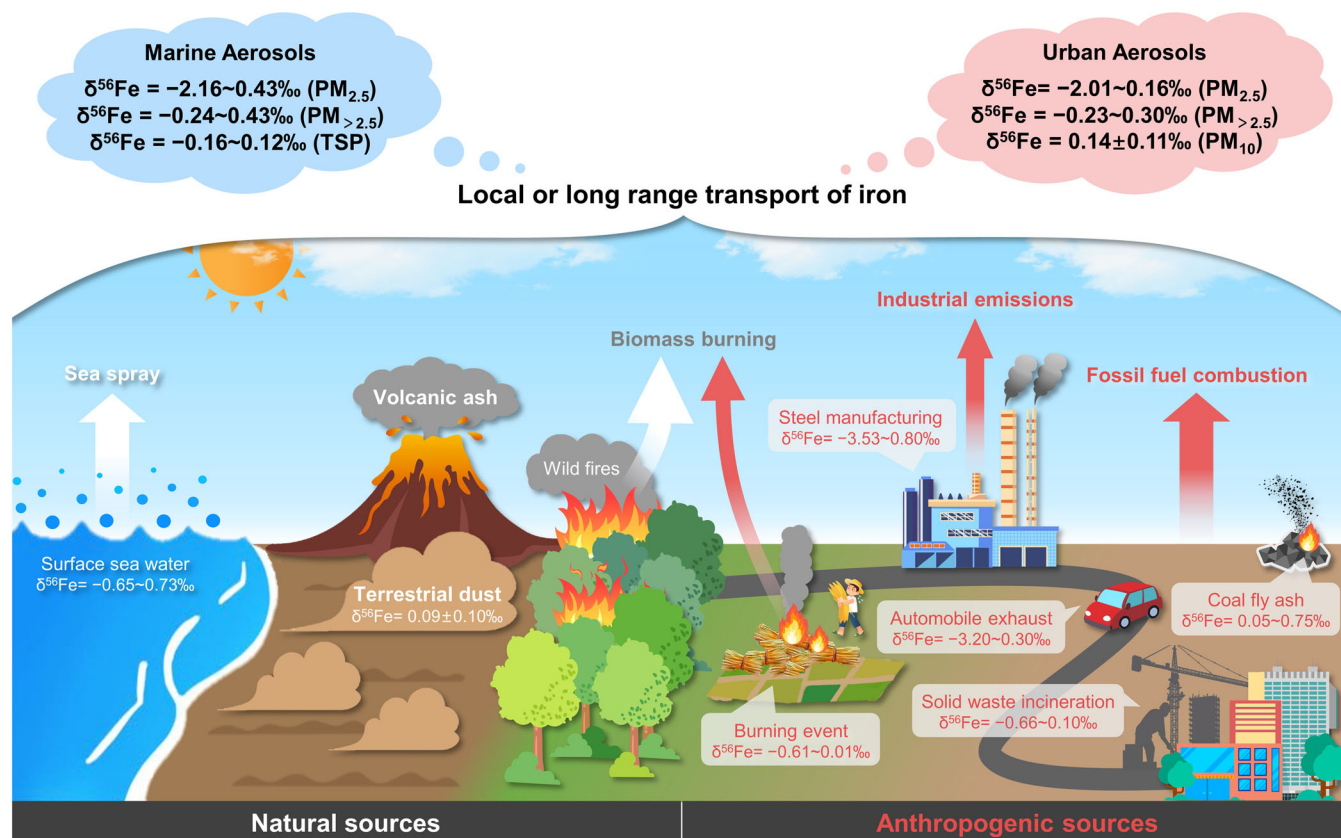

Fig. 5   Graphical illustration of the emission from natural and anthropogenic sources to atmospheric iron. The δ^{56}Fe values of iron sources, including surface sea water[52,134], terrestrial dust[125], burning event[140], steel manufacturing[142,147], coal fly ash[128,146], solid waste incineration[141,146] and exhausted gasoline[141], are according to published literature (There are no data for volcanic ash and wild fires, etc.). Iron isotopic variations in both fine and coarse particles in marine[71,127,128,148,152,155] and urban aerosols[147,148,150] are also listed.

4. More attention should be paid to the source apportionment by the use of different mathematical models. Here we applied a Bayesian isotope mixing model MixSIAR with stable iron isotopes to quantitatively calculate the contribution of different iron sources. The method can be applied in different background aerosols, to verify its practicality in a wider range of regions, although the reliability of the results

needs further verification, which calls for further development of effective models.

5. Metal stable isotopes such as δ^{56}Fe could serve as valuable references to identify sources of atmospheric aerosols. It is necessary to conduct such studies in developing countries such as China and India, where air pollution[161] is largely caused by rapid industrialization.

Successful studies of iron stable isotopes in the atmosphere have shed light on their valuable use in source apportionment, providing significant insights into the biogeochemical cycles of iron at the land–ocean–atmosphere interfaces. Undoubtedly, metal stable isotope analyses have emerged as a powerful tool in both source tracing and elucidating biogeochemical cycles of trace elements such as Fe, Cu, Zn, Mg, and Hg. Our understanding of the application of metal stable isotopes in atmospheric chemistry remains in an early stage and is still incomplete, with many questions remaining open for future studies.

DATA AVAILABILITY

Derived data in this study are available from the corresponding author upon reasonable request.

REFERENCES

1. Li, Z. Q. et al. Aerosol and boundary-layer interactions and impact on air quality. *Natl Sci. Rev.* **4**, 810–833 (2017).
2. Reddy, M. S. & Venkataraman, C. Atmospheric optical and radiative effects of anthropogenic aerosol constituents from India. *Atmos. Environ.* **34**, 4511–4523 (2000).
3. Cohen, A. J. et al. Estimates and 25-year trends of the global burden of disease attributable to ambient air pollution: an analysis of data from the Global Burden of Diseases Study 2015. *Lancet* **389**, 1907–1918 (2017).
4. Lelieveld, J., Evans, J. S., Fnais, M., Giannadaki, D. & Pozzer, A. The contribution of outdoor air pollution sources to premature mortality on a global scale. *Nature* **525**, 367–371 (2015).
5. Carslaw, K. S. et al. A review of natural aerosol interactions and feedbacks within the Earth system. *Atmos. Chem. Phys.* **10**, 1701–1737 (2010).
6. Fuzzi, S. et al. Particulate matter, air quality and climate: lessons learned and future needs. *Atmos. Chem. Phys.* **15**, 8217–8299 (2015).
7. Huang, S. et al. Overview of biological ice nucleating particles in the atmosphere. *Environ. Int.* **146**, 106197 (2021).
8. An, Z. et al. Severe haze in northern China: a synergy of anthropogenic emissions and atmospheric processes. *Proc. Natl Acad. Sci. USA* **116**, 8657–8666 (2019).
9. Chan, C. K. & Yao, X. Air pollution in mega cities in China. *Atmos. Environ.* **42**, 1–42 (2008).
10. Mahowald, N. M. et al. Aerosol trace metal leaching and impacts on marine microorganisms. *Nat. Commun.* **9**, 2614 (2018).
11. Fang, G. C., Huang, Y. L. & Huang, J. H. Study of atmospheric metallic elements pollution in Asia during 2000–2007. *J. Hazard. Mater.* **180**, 115–121 (2010).
12. Duan, J. C. & Tan, J. H. Atmospheric heavy metals and arsenic in China: situation, sources and control policies. *Atmos. Environ.* **74**, 93–101 (2013).
13. Kappler, A. & Straub, K. L. Geomicrobiological cycling of iron. *Rev. Mineral. Geochem.* **59**, 85–108 (2005).
14. Kappler, A. et al. An evolving view on biogeochemical cycling of iron. *Nat. Rev. Microbiol.* **19**, 360–374 (2021).
15. Tagliabue, A. et al. The integral role of iron in ocean biogeochemistry. *Nature* **543**, 51–59 (2017).
16. Martin, J. H., Fitzwater, S. E. & Gordon, R. M. Iron deficiency limits phytoplankton growth in Antarctic waters. *Global Biogeochem. Cycles* **4**, 5–12 (1990).
17. Smetacek, V. et al. Deep carbon export from a Southern Ocean iron-fertilized diatom bloom. *Nature* **487**, 313–319 (2012).
18. Martin, J. H., Gordon, M. & Fitzwater, S. E. The case for iron. *Limnol. Oceanogr.* **36**, 1793–1802 (1991).
19. Martin, J. H. Glacial-interglacial CO$_2$ change: the iron hypothesis. *Paleoceanography* **5**, 1–13 (1990).
20. Walczyk, T. & von Blanckenburg, F. Natural iron isotope variations in human blood. *Science* **295**, 2065–2066 (2002).
21. Valdiglesias, V. et al. Effects of iron oxide nanoparticles: cytotoxicity, genotoxicity, developmental toxicity, and neurotoxicity. *Environ. Mol. Mutagen.* **56**, 125–148 (2015).
22. Lu, D. et al. Chemical multi-fingerprinting of exogenous ultrafine particles in human serum and pleural effusion. *Nat. Commun.* **11**, 2567 (2020).
23. Maher, B. A. et al. Magnetite pollution nanoparticles in the human brain. *Proc. Natl Acad. Sci. USA* **113**, 10797–10801 (2016).
24. Lam, P. J. & Bishop, J. K. B. The continental margin is a key source of iron to the HNLC North Pacific Ocean. *Geophys. Res. Lett.* **35**, L07608 (2008).
25. Raiswell, R., Benning, L. G., Tranter, M. & Tulaczyk, S. Bioavailable iron in the Southern Ocean: the significance of the iceberg conveyor belt. *Geochem. Trans.* **9**, 7 (2008).
26. Crusius, J. et al. Glacial flour dust storms in the Gulf of Alaska: hydrologic and meteorological controls and their importance as a source of bioavailable iron. *Geophys. Res. Lett.* **38**, L06602 (2011).
27. Tagliabue, A. et al. Hydrothermal contribution to the oceanic dissolved iron inventory. *Nat. Geosci.* **3**, 252–256 (2010).
28. Jickells, T. D. et al. Global iron connections between desert dust, ocean biogeochemistry, and climate. *Science* **308**, 67–71 (2005).
29. Jickells, T. & Moore, C. M. The importance of atmospheric deposition for ocean productivity. *Annu. Rev. Ecol. Evol. Syst.* **46**, 481–501 (2015).
30. Mahowald, N. M. et al. Atmospheric global dust cycle and iron inputs to the ocean. *Global Biogeochem. Cycles* **19**, GB4025 (2005).
31. Calvo, A. I. et al. Research on aerosol sources and chemical composition: Past, current and emerging issues. *Atmos. Res.* **120**, 1–28 (2013).
32. Choobari, O. A., Zawar-Reza, P. & Sturman, A. The global distribution of mineral dust and its impacts on the climate system: a review. *Atmos. Res.* **138**, 152–165 (2014).
33. Tegen, I., Werner, M., Harrison, S. P. & Kohfeld, K. E. Relative importance of climate and land use in determining present and future global soil dust emission. *Geophys. Res. Lett.* **31**, L05105 (2004).
34. Textor, C. et al. Analysis and quantification of the diversities of aerosol life cycles within AeroCom. *Atmos. Chem. Phys.* **6**, 1777–1813 (2006).
35. Hamilton, D. S. et al. Earth, wind, fire, and pollution: aerosol nutrient sources and impacts on ocean biogeochemistry. *Annu. Rev. Mar. Sci.* **14**, 11.11–11.28 (2022).
36. Lighty, J. S., Veranth, J. M. & Sarofim, A. F. Combustion aerosols: factors governing their size and composition and implications to human health. *J. Air Waste Manage. Assoc.* **50**, 1619–1622 (2000).
37. Harrison, R. M. et al. Non-exhaust vehicle emissions of particulate matter and VOC from road traffic: a review. *Atmos. Environ.* **262**, 118592 (2021).
38. Yue, S. et al. Brown carbon from biomass burning imposes strong circum-Arctic warming. *One Earth* **5**, 293–304 (2022).
39. Shi, Z. B. et al. Impacts on iron solubility in the mineral dust by processes in the source region and the atmosphere: a review. *Aeol. Res.* **5**, 21–42 (2012).
40. Baker, A. R. & Jickells, T. D. Mineral particle size as a control on aerosol iron solubility. *Geophys. Res. Lett.* **33**, L17608 (2006).
41. Shi, Z. B. et al. Minor effect of physical size sorting on iron solubility of transported mineral dust. *Atmos. Chem. Phys.* **11**, 8459–8469 (2011).
42. Takahashi, Y., Higashi, M., Furukawa, T. & Mitsunobu, S. Change of iron species and iron solubility in Asian dust during the long-range transport from western China to Japan. *Atmos. Chem. Phys.* **11**, 11237–11252 (2011).
43. Johnson, M. S. & Meskhidze, N. Atmospheric dissolved iron deposition to the global oceans: effects of oxalate-promoted Fe dissolution, photochemical redox cycling, and dust mineralogy. *Geosci. Model Dev.* **6**, 1137–1155 (2013).
44. Longo, A. F. et al. Influence of atmospheric processes on the solubility and composition of iron in Saharan dust. *Environ. Sci. Technol.* **50**, 6912–6920 (2016).
45. Baker, A. R. et al. Changing atmospheric acidity as a modulator of nutrient deposition and ocean biogeochemistry. *Sci. Adv.* **7**, eabd8800 (2021).
46. Li, W. et al. Air pollution–aerosol interactions produce more bioavailable iron for ocean ecosystems. *Sci. Adv.* **3**, e1601749 (2017).
47. Zhang, H. et al. Abundance and fractional solubility of aerosol iron during winter at a coastal city in Northern China: similarities and contrasts between fine and coarse particles. *J. Geophys. Res. Atmos.* **127**, e2021JD036070 (2022).
48. Paris, R., Desboeufs, K. V., Formenti, P., Nava, S. & Chou, C. Chemical characterisation of iron in dust and biomass burning aerosols during AMMA-SOP0/DABEX: implication for iron solubility. *Atmos. Chem. Phys.* **10**, 4273–4282 (2010).
49. Paris, R. & Desboeufs, K. V. Effect of atmospheric organic complexation on iron-bearing dust solubility. *Atmos. Chem. Phys.* **13**, 4895–4905 (2013).
50. Moore, J. K. & Braucher, O. Sedimentary and mineral dust sources of dissolved iron to the world ocean. *Biogeosciences* **5**, 631–656 (2008).
51. Ito, A., Ye, Y., Baldo, C. & Shi, Z. Ocean fertilization by pyrogenic aerosol iron. *npj Clim. Atmos. Sci.* **4**, 30 (2021).
52. Pinedo-Gonzalez, P. et al. Anthropogenic Asian aerosols provide Fe to the North Pacific Ocean. *Proc. Natl Acad. Sci. USA* **117**, 27862–27868 (2020).
53. Lamb, K. D. et al. Global-scale constraints on light-absorbing anthropogenic iron oxide aerosols. *npj Clim. Atmos. Sci.* **4**, 15 (2021).
54. Liu, M. et al. The underappreciated role of anthropogenic sources in atmospheric soluble iron flux to the Southern Ocean. *npj Clim. Atmos. Sci.* **5**, 28 (2022).

55. Hamilton, D. S. et al. Recent (1980 to 2015) trends and variability in daily-to-interannual soluble iron deposition from dust, fire, and anthropogenic sources. *Geophys. Res. Lett.* **47**, e2020GL089688 (2020).

56. Hamilton, D. S. et al. Impact of changes to the atmospheric soluble iron deposition flux on ocean biogeochemical cycles in the Anthropocene. *Global Biogeochem. Cycles* **34**, e2019GB006448 (2020).

57. Ito, A. & Shi, Z. Delivery of anthropogenic bioavailable iron from mineral dust and combustion aerosols to the ocean. *Atmos. Chem. Phys.* **16**, 85–99 (2016).

58. Chuang, P. Y., Duvall, R. M., Shafer, M. M. & Schauer, J. J. The origin of water soluble particulate iron in the Asian atmospheric outflow. *Geophys. Res. Lett.* **32**, L07813 (2005).

59. Guieu, C., Bonnet, S., Wagener, T. & Loÿe-Pilot, M.-D. Biomass burning as a source of dissolved iron to the open ocean? *Geophys. Res. Lett.* **32**, L19608 (2005).

60. Sedwick, P. N., Sholkovitz, E. R. & Church, T. M. Impact of anthropogenic combustion emissions on the fractional solubility of aerosol iron: evidence from the Sargasso Sea. *Geochem. Geophys. Geosyst.* **8**, Q10Q06 (2007).

61. Luo, C. et al. Combustion iron distribution and deposition. *Global Biogeochem. Cycles* **22**, GB1012 (2008).

62. Sholkovitz, E. R., Sedwick, P. N. & Church, T. M. Influence of anthropogenic combustion emissions on the deposition of soluble aerosol iron to the ocean: empirical estimates for island sites in the North Atlantic. *Geochim. Cosmochim. Acta* **73**, 3981–4003 (2009).

63. Ito, A. Atmospheric processing of combustion aerosols as a source of bioavailable iron. *Environ. Sci. Technol. Lett.* **2**, 70–75 (2015).

64. Schroth, A. W., Crusius, J., Sholkovitz, E. R. & Bostick, B. C. Iron solubility driven by speciation in dust sources to the ocean. *Nat. Geosci.* **2**, 337–340 (2009).

65. Zhu, Y. et al. Iron solubility in fine particles associated with secondary acidic aerosols in east China. *Environ. Pollut.* **264**, 114769 (2020).

66. Ito, A., Ye, Y., Yamamoto, A., Watanabe, M. & Aita, M. N. Responses of ocean biogeochemistry to atmospheric supply of lithogenic and pyrogenic iron-containing aerosols. *Geol. Mag.* **157**, 741–756 (2019).

67. Ito, A. et al. Evaluation of aerosol iron solubility over Australian coastal regions based on inverse modeling: implications of bushfires on bioaccessible iron concentrations in the Southern Hemisphere. *Prog. Earth Plant. Sci.* **7**, 42 (2020).

68. Sholkovitz, E. R., Sedwick, P. N., Church, T. M., Baker, A. R. & Powell, C. F. Fractional solubility of aerosol iron: synthesis of a global-scale data set. *Geochim. Cosmochim. Acta* **89**, 173–189 (2012).

69. Ito, A. et al. Pyrogenic iron: the missing link to high iron solubility in aerosols. *Sci. Adv.* **5**, eaau7671 (2019).

70. Trapp, J. M., Millero, F. J. & Prospero, J. M. Trends in the solubility of iron in dust-dominated aerosols in the equatorial Atlantic trade winds: Importance of iron speciation and sources. *Geochem. Geophys. Geosyst.* **11**, Q03014 (2010).

71. Conway, T. M. et al. Tracing and constraining anthropogenic aerosol iron fluxes to the North Atlantic Ocean using iron isotopes. *Nat. Commun.* **10**, 2628 (2019).

72. Du, Z. et al. The iron records and its sources during 1990–2017 from the Lambert Glacial Basin shallow ice core, East Antarctica. *Chemosphere* **251**, 126399 (2020).

73. Conway, T. M., Wolff, E. W., Rothlisberger, R., Mulvaney, R. & Elderfield, H. E. Constraints on soluble aerosol iron flux to the Southern Ocean at the Last Glacial Maximum. *Nat. Commun.* **6**, 7850 (2015).

74. Zhu, Y. et al. Sources and processes of iron aerosols in a megacity in Eastern China. *Atmos. Chem. Phys.* **22**, 2191–2202 (2022).

75. Hoefs, J. *Stable Isotope Geochemistry* (Springer, 2018).

76. White, W. M. *Isotope Geochemistry* (John Wiley & Sons, 2015).

77. Michener, R. & Lajtha, K. *Stable Isotopes in Ecology and Environmental Science* (Blackwell, 2007).

78. Dawson, T. E., Mambelli, S., Plamboeck, A. H., Templer, P. H. & Tu, K. P. Stable isotopes in plant ecology. *Annu. Rev. Ecol. Syst.* **33**, 507–559 (2002).

79. Caut, S., Angulo, E. & Courchamp, F. Variation in discrimination factors (Δ^{15}N and Δ^{13}C): the effect of diet isotopic values and applications for diet reconstruction. *J. Appl. Ecol.* **46**, 443–453 (2009).

80. Parnell, A. C., Inger, R., Bearhop, S. & Jackson, A. L. Source partitioning using stable isotopes: coping with too much variation. *PLoS ONE* **5**, e9672 (2010).

81. Wu, L. B. et al. Aerosol ammonium in the urban boundary layer in Beijing: insights from nitrogen isotope ratios and simulations in summer 2015. *Environ. Sci. Technol. Lett.* **6**, 389–395 (2019).

82. Wu, L. et al. Source forensics of inorganic and organic nitrogen using δ^{15}N for tropospheric aerosols over Mt. Tai. *npj Clim. Atmos. Sci.* **4**, 8 (2021).

83. Han, X. et al. Multiple sulfur isotope constraints on sources and formation processes of sulfate in Beijing PM$_{2.5}$ aerosol. *Environ. Sci. Technol* **51**, 7794–7803 (2017).

84. López-Veneroni, D. The stable carbon isotope composition of PM$_{2.5}$ and PM$_{10}$ in Mexico City Metropolitan Area air. *Atmos. Environ.* **43**, 4491–4502 (2009).

85. Zhao, W. et al. Molecular distribution and compound-specific stable carbon isotopic composition of dicarboxylic acids, oxocarboxylic acids and α-dicarbonyls in PM$_{2.5}$ from Beijing, China. *Atmos. Chem. Phys.* **18**, 2749–2767 (2018).

86. Weiss, D. J. et al. Application of nontraditional stable-isotope systems to the study of sources and fate of metals in the environment. *Environ. Sci. Technol.* **42**, 655–664 (2008).

87. Wiederhold, J. G. Metal stable isotope signatures as tracers in environmental geochemistry. *Environ. Sci. Technol.* **49**, 2606–2624 (2015).

88. Anbar, A. D., Jarzecki, A. A. & Spiro, T. G. Theoretical investigation of iron isotope fractionation between Fe(H$_2$O)$_6$$^{3+}$ and Fe(H$_2$O)$_6$$^{2+}$: implications for iron stable isotope geochemistry. *Geochim. Cosmochim. Acta* **69**, 825–837 (2005).

89. Welch, S. A., Beard, B. L., Johnson, C. M. & Braterman, P. S. Kinetic and equilibrium Fe isotope fractionation between aqueous Fe(II) and Fe(III). *Geochim. Cosmochim. Acta* **67**, 4231–4250 (2003).

90. Wiederhold, J. G., Kraemer, S. M., Teutsch, N., Borer, P. M. & Kretzschmar, R. Iron isotope fractionation during proton-promoted, ligand-controlled, and reductive dissolution of goethite. *Environ. Sci. Technol.* **40**, 3787–3793 (2006).

91. Chapman, J. B., Weiss, D. J., Shan, Y. & Lemburger, M. Iron isotope fractionation during leaching of granite and basalt by hydrochloric and oxalic acids. *Geochim. Cosmochim. Acta* **73**, 1312–1324 (2009).

92. Richter, F. M., Dauphas, N. & Teng, F. Z. Non-traditional fractionation of non-traditional isotopes: evaporation, chemical diffusion and Soret diffusion. *Chem. Geol.* **258**, 92–103 (2009).

93. Kiczka, M., Wiederhold, J. G., Kraemer, S. M., Bourdon, B. & Kretzschmar, R. Iron isotope fractionation during Fe uptake and translocation in alpine plants. *Environ. Sci. Technol.* **44**, 6144–6150 (2010).

94. Estrade, N., Carignan, J. & Donard, O. Isotope tracing of atmospheric mercury sources in an urban area of northeastern France. *Environ. Sci. Technol.* **44**, 6062 (2010).

95. Chen, J., Gaillardet, J. & Louvat, P. Zinc isotopes in the Seine River waters, France: a probe of anthropogenic contamination. *Environ. Sci. Technol.* **42**, 6494–6501 (2008).

96. Albarède, F. et al. Precise and accurate isotopic measurements using multiple-collector ICPMS. *Geochim. Cosmochim. Acta* **68**, 2725–2744 (2004).

97. Maréchal, C. N., Télouk, P. & Albarède, F. Precise analysis of copper and zinc isotopic compositions by plasma-source mass spectrometry. *Chem. Geol.* **156**, 251–273 (1999).

98. Araújo, D. F. et al. Tracing of anthropogenic zinc sources in coastal environments using stable isotope composition. *Chem. Geol.* **449**, 226–235 (2017).

99. Desaulty, A. M. & Petelet-Giraud, E. Zinc isotope composition as a tool for tracing sources and fate of metal contaminants in rivers. *Sci. Total Environ.* **728**, 138599 (2020).

100. Li, H. Y. et al. Rapid transition in winter aerosol composition in Beijing from 2014 to 2017: response to clean air actions. *Atmos. Chem. Phys.* **19**, 11485–11499 (2019).

101. Li, W. et al. Environmental applications of metal stable isotopes: silver, mercury and zinc. *Atmos. Environ.* **252**, 1344–1356 (2019).

102. Widory, D., Liu, X. & Dong, S. Isotopes as tracers of sources of lead and strontium in aerosols (TSP & PM$_{2.5}$) in Beijing. *Atmos. Environ.* **44**, 3679–3687 (2010).

103. Zhao, L. S. et al. Source apportionment of heavy metals in urban road dust in a continental city of eastern China: using Pb and Sr isotopes combined with multivariate statistical analysis. *Atmos. Environ.* **201**, 201–211 (2019).

104. Zhao, Z. Q. et al. Atmospheric lead in urban Guiyang, Southwest China: isotopic source signatures. *Atmos. Environ.* **115**, 163–169 (2015).

105. Lu, D. et al. Natural silicon isotopic signatures reveal the sources of airborne fine particulate matter. *Environ. Sci. Technol.* **52**, 1088–1095 (2018).

106. Yang, X. et al. Two-dimensional silicon fingerprints reveal dramatic variations in the sources of particulate matter in Beijing during 2013–2017. *Environ. Sci. Technol.* **54**, 7126–7135 (2020).

107. Huang, Q. et al. Isotopic composition for source identification of mercury in atmospheric fine particles. *Atmos. Chem. Phys.* **16**, 11773–11786 (2016).

108. Xu, H. M. et al. Mercury stable isotope compositions of Chinese urban fine particulates in winter haze days: implications for Hg sources and transformations. *Chem. Geol.* **504**, 267–275 (2019).

109. Jiskra, M. et al. Mercury stable isotopes constrain atmospheric sources to the ocean. *Nature* **597**, 678–682 (2021).

110. Gonzalez, R. O. et al. New insights from zinc and copper isotopic compositions into the sources of atmospheric particulate matter from two major European cities. *Environ. Sci. Technol.* **50**, 9816–9824 (2016).

111. Dauphas, N., John, S. G. & Rouxel, O. Iron isotope systematics. *Rev. Mineral. Geochem.* **82**, 415–510 (2017).

112. Johnson, C. M., Beard, B. L. & Roden, E. E. The iron isotope fingerprints of redox and biogeochemical cycling in the modern and ancient Earth. *Annu. Rev. Earth Planet. Sci.* **36**, 457–493 (2008).

113. Zhang, R. et al. Iron isotope biogeochemical cycling in the Western Arctic Ocean. *Global Biogeochem. Cycles* **35**, e2021GB006977 (2021).

114. Bergquist, B. A. & Boyle, E. A. Iron isotopes in the Amazon River system: weathering and transport signatures. *Earth Planet. Sci. Lett.* **248**, 54–68 (2006).

115. Wu, B., Amelung, W., Xing, Y., Bol, R. & Berns, A. E. Iron cycling and isotope fractionation in terrestrial ecosystems. *Earth-Sci. Rev.* **190**, 323–352 (2019).

116. Huang, L. M. et al. Variations and controls of iron oxides and isotope compositions during paddy soil evolution over a millennial time scale. *Chem. Geol.* **476**, 340–351 (2018).

117. Qi, Y. H. et al. Iron stable isotopes in bulk soil and sequential extracted fractions trace Fe redox cycling in paddy soils. *J. Argric. Food Chem.* **68**, 8143–8150 (2020).

118. Albarède, F. Metal stable isotopes in the human body: a tribute of geochemistry to medicine. *Elements* **11**, 265–269 (2015).

119. Krayenbuehl, P. A., Walczyk, T., Schoenberg, R., von Blanckenburg, F. & Schulthess, G. Hereditary hemochromatosis is reflected in the iron isotope composition of blood. *Blood* **105**, 3812–3816 (2005).

120. Beard, B. L. & Johnson, C. M. High precision iron isotope measurements of terrestrial and lunar materials. *Geochim. Cosmochim. Acta* **63**, 1653–1660 (1999).

121. Rouxel, O., Dobbek, N., Ludden, J. & Fouquet, Y. Iron isotope fractionation during oceanic crust alteration. *Chem. Geol.* **202**, 155–182 (2003).

122. Beard, B. L., Johnson, C. M., Damm, K. V. & Poulson, R. L. Iron isotope constraints on Fe cycling and mass balance in oxygenated Earth oceans. *Geology* **31**, 629–632 (2003).

123. Heimann, A., Beard, B. L. & Johnson, C. M. The role of volatile exsolution and sub-solidus fluid/rock interactions in producing high $^{56}Fe/^{54}Fe$ ratios in siliceous igneous rocks. *Geochim. Cosmochim. Acta* **72**, 4379–4396 (2008).

124. Fantle, M. S. & DePaolo, D. J. Iron isotopic fractionation during continental weathering. *Earth Planet. Sci. Lett.* **228**, 547–562 (2004).

125. Beard, B. L. et al. Application of Fe isotopes to tracing the geochemical and biological cycling of Fe. *Chem. Geol.* **195**, 87–117 (2003).

126. Poitrasson, F. On the iron isotope homogeneity level of the continental crust. *Chem. Geol.* **235**, 195–200 (2006).

127. Waeles, M., Baker, A. R., Jickells, T. & Hoogewerff, J. Global dust teleconnections: aerosol iron solubility and stable isotope composition. *Environ. Chem.* **4**, 233–237 (2007).

128. Mead, C., Herckes, P., Majestic, B. J. & Anbar, A. D. Source apportionment of aerosol iron in the marine environment using iron isotope analysis. *Geophys. Res. Lett.* **40**, 5722–5727 (2013).

129. Grythe, H., Strom, J., Krejci, R., Quinn, P. & Stohl, A. A review of sea-spray aerosol source functions using a large global set of sea salt aerosol concentration measurements. *Atmos. Chem. Phys.* **14**, 1277–1297 (2014).

130. Gong, S. L., Barrie, L. A. & Lazare, M. Canadian Aerosol Module (CAM): a size-segregated simulation of atmospheric aerosol processes for climate and air quality models—2. Global sea-salt aerosol and its budgets. *J. Geophys. Res. Atmos.* **107**, 4779 (2002).

131. Olgun, N. et al. Surface ocean iron fertilization: the role of airborne volcanic ash from subduction zone and hot spot volcanoes and related iron fluxes into the Pacific Ocean. *Global Biogeochem. Cycles* **25**, GB4001 (2011).

132. Duggen, S., Croot, P., Schacht, U. & Hoffmann, L. Subduction zone volcanic ash can fertilize the surface ocean and stimulate phytoplankton growth: evidence from biogeochemical experiments and satellite data. *Geophys. Res. Lett.* **34**, L01612 (2007).

133. Hamme, R. C. et al. Volcanic ash fuels anomalous plankton bloom in subarctic northeast Pacific. *Geophys. Res. Lett.* **37**, L19604 (2010).

134. Conway, T. M. & John, S. G. Quantification of dissolved iron sources to the North Atlantic Ocean. *Nature* **511**, 212–215 (2014).

135. Ellwood, M. J. et al. Iron stable isotopes track pelagic iron cycling during a subtropical phytoplankton bloom. *Proc. Natl Acad. Sci. USA* **112**, E15–E20 (2015).

136. Chen, J. et al. A review of biomass burning: emissions and impacts on air quality, health and climate in China. *Sci. Total Environ.* **579**, 1000–1034 (2017).

137. Streets, D. G., Yarber, K. F., Woo, J. H. & Carmichael, G. R. Biomass burning in Asia: annual and seasonal estimates and atmospheric emissions. *Global Biogeochem. Cycles* **17**, 1099 (2003).

138. Guelke, M. & Von Blanckenburg, F. Fractionation of stable iron isotopes in higher plants. *Environ. Sci. Technol.* **41**, 1896–1901 (2007).

139. Winton, V. H. L. et al. Dry season aerosol iron solubility in tropical northern Australia. *Atmos. Chem. Phys.* **16**, 12829–12848 (2016).

140. Kurisu, M. & Takahashi, Y. Testing iron stable isotope ratios as a signature of biomass burning. *Atmosphere* **10**, 76 (2019).

141. Kurisu, M. et al. Variation of iron isotope ratios in anthropogenic materials emitted through combustion processes. *Chem. Lett.* **45**, 970–972 (2016).

142. Kurisu, M., Adachi, K., Sakata, K. & Takahashi, Y. Stable isotope ratios of combustion iron produced by evaporation in a steel plant. *ACS Earth Space Chem.* **3**, 588–598 (2019).

143. Majestic, B. J., Anbar, A. D. & Herckes, P. Elemental and iron isotopic composition of aerosols collected in a parking structure. *Sci. Total Environ.* **407**, 5104–5109 (2009).

144. Jung, C. H., Matsuto, T., Tanaka, N. & Okada, T. Metal distribution in incineration residues of municipal solid waste (MSW) in Japan. *Waste Manag.* **24**, 381–391 (2004).

145. Wei, Y., Shimaoka, T., Saffarzadeh, A. & Takahashi, F. Mineralogical characterization of municipal solid waste incineration bottom ash with an emphasis on heavy metal-bearing phases. *J. Hazard. Mater.* **187**, 534–543 (2011).

146. Li, R. et al. Mass fractions, solubility, speciation and isotopic compositions of iron in coal and municipal waste fly ash. *Sci. Total Environ.* **838**, 155974 (2022).

147. Flament, P. et al. Iron isotopic fractionation in industrial emissions and urban aerosols. *Chemosphere* **73**, 1793–1798 (2008).

148. Kurisu, M., Takahashi, Y., Iizuka, T. & Uematsu, M. Very low isotope ratio of iron in fine aerosols related to its contribution to the surface ocean. *J. Geophys. Res. Atmos.* **121**, 11119–11136 (2016).

149. Beddows, D. C. S. & Harrison, R. M. Identification of specific sources of airborne particles emitted from within a complex industrial (steelworks) site. *Atmos. Environ.* **183**, 122–134 (2018).

150. Majestic, B. J., Anbar, A. D. & Herckes, P. Stable isotopes as a tool to apportion atmospheric iron. *Environ. Sci. Technol.* **43**, 4327–4333 (2009).

151. Zuo, P. et al. Stable iron isotopic signature reveals multiple sources of magnetic particulate matter in the 2021 Beijing sandstorms. *Environ. Sci. Technol. Lett.* **9**, 299–305 (2022).

152. Kurisu, M., Sakata, K., Uematsu, M., Ito, A. & Takahashi, Y. Contribution of combustion Fe in marine aerosols over the northwestern Pacific estimated by Fe stable isotope ratios. *Atmos. Chem. Phys.* **21**, 16027–16050 (2021).

153. Furutani, H. et al. Single-particle chemical characterization and source apportionment of iron-containing atmospheric aerosols in Asian outflow. *J. Geophys. Res. Atmos.* **116**, D18204 (2011).

154. Ito, A. Global modeling study of potentially bioavailable iron input from shipboard aerosol sources to the ocean. *Global Biogeochem. Cycles* **27**, 1–10 (2013).

155. Labatut, M. et al. Iron sources and dissolved-particulate interactions in the seawater of the Western Equatorial Pacific, iron isotope perspectives. *Global Biogeochem. Cycles* **28**, 1044–1065 (2014).

156. Radic, A., Lacan, F. & Murray, J. W. Iron isotopes in the seawater of the equatorial Pacific Ocean: new constraints for the oceanic iron cycle. *Earth Planet. Sci. Lett.* **306**, 1–10 (2011).

157. Stock, B. C. et al. Analyzing mixing systems using a new generation of Bayesian tracer mixing models. *PeerJ* **6**, e5096 (2018).

158. Stock, B. & Semmens, B. *MixSIAR GUI User Manual, Version 3.1* https://github.com/brianstock/MixSIAR/ (2018).

159. Parnell, A. C. et al. Bayesian stable isotope mixing models. *Environmetrics* **24**, 387–399 (2013).

160. Souto-Oliveira, C. E., Babinski, M., Araujo, D. F. & Andrade, M. F. Multi-isotopic fingerprints (Pb, Zn, Cu) applied for urban aerosol source apportionment and discrimination. *Sci. Total Environ.* **626**, 1350–1366 (2018).

161. Zhang, Y. L. & Cao, F. Fine particulate matter ($PM_{2.5}$) in China at a city level. *Sci. Rep.* **5**, 14884 (2015).

162. Thompson, A., Ruiz, J., Chadwick, O. A., Titus, M. & Chorover, J. Rayleigh fractionation of iron isotopes during pedogenesis along a climate sequence of Hawaiian basalt. *Chem. Geol.* **238**, 72–83 (2007).

163. Gong, Y., Xia, Y., Huang, F. & Yu, H. Average iron isotopic compositions of the upper continental crust: constrained by loess from the Chinese Loess Plateau. *Acta Geochim.* **36**, 125–131 (2017).

164. Zhu, X.-K., O'Nions, R. K., Guo, Y. & Reynolds, B. C. Secular variation of iron isotopes in North Atlantic deep water. *Science* **287**, 2000–2002 (2000).

165. John, S. G. & Adkins, J. The vertical distribution of iron stable isotopes in the North Atlantic near Bermuda. *Global Biogeochem. Cycles* **26**, GB2034 (2012).

ACKNOWLEDGEMENTS

AUTHOR CONTRIBUTIONS
P.F. proposed the concept and supervised. Y.W. and L.W. wrote the draft and conducted model calculations. All authors contributed to revising and finalizing the manuscript.

COMPETING INTERESTS
R.M.H. is co-editor-in-chief, and P.F. is associate editor of *npj Climate and Atmospheric Science*. They were not involved in the journal's review of or decisions related to this manuscript. The authors declare no competing interests.

ADDITIONAL INFORMATION

Supplementary information The online version contains supplementary material available at https://doi.org/10.1038/s41612-022-00299-7.

Correspondence and requests for materials should be addressed to Pingqing Fu.

Reprints and permission information is available at http://www.nature.com/reprints

Publisher's note Springer Nature remains neutral with regard to jurisdictional claims in published maps and institutional affiliations.